Fullerene-like WS_2 supported Pd catalyst for hydrogen evolution reaction

Xiao, Ping; Buijnsters, Josephus G.; Zhao, Yanxi; Yu, Huan; Xu, Xuelian; Zhu, Yujun; Tang, Duihai; Zhu, Junjiang; Zhao, Zhen

DOI
10.1016/j.jcat.2019.10.007

Publication date
2019

Document Version
Final published version

Published in
Journal of Catalysis

Journal of Catalysis 380 (2019) 215–223

Contents lists available at ScienceDirect

Journal of Catalysis

journal homepage: www.elsevier.com/locate/jcat

Fullerene-like WS_2 supported Pd catalyst for hydrogen evolution reaction

Ping Xiao [a,b,1], Josephus G. Buijnsters [c,1], Yanxi Zhao [d], Huan Yu [e], Xuelian Xu [a,e], Yujun Zhu [b], Duihai Tang [e], Junjiang Zhu [a,e,*], Zhen Zhao [e]

[a] Hubei Key Laboratory of Biomass Fibers and Eco-dyeing & Finishing, College of Chemistry and Chemical Engineering, Wuhan Textile University, Wuhan 430200, PR China
[b] Key Laboratory of Functional Inorganic Material Chemistry (Heilongjiang University), Ministry of Education, School of Chemistry and Materials, Heilongjiang University, Harbin 150080, PR China
[c] Department of Precision and Microsystems Engineering, Research Group of Micro and Nano Engineering, Delft University of Technology, Mekelweg 2, 2628 CD Delft, The Netherlands
[d] Key Laboratory of Catalysis and Materials Science of the State Ethnic Affairs & Commission Ministry of Education, College of Chemistry and Materials Science, South-Central University for Nationalities, Wuhan 430200, PR China
[e] Institute of Catalysis for Energy and Environment, College of Chemistry and Chemical Engineering, Shenyang Normal University, Shenyang 110034, PR China

ARTICLE INFO

Article history:
Received 25 June 2019
Revised 30 September 2019
Accepted 7 October 2019
Available online 31 October 2019

Keywords:
Electrocatalytic hydrogen evolution
Tungsten disulfide
Palladium catalyst
Tungsten trioxide
Reaction mechanism

ABSTRACT

Hydrogen is the most desirable green energy carrier and electrocatalytic hydrogen evolution reaction (HER) from water is a promising route for hydrogen production. The search for efficient, low-cost HER catalysts is a challenging and attracting topic. In this work, we report that inorganic fullerene-like WS_2 supported Pd nanoparticles (Pd/WS_2), with Pd loading of 0.76 wt%, are active for electrocatalytic HER conducted in 0.5 M H_2SO_4 solution, with overpotential at 10 mA cm^{-2} current density of ~130 mV and Tafel slope of 82.4 mV dec^{-1}, which is comparable to that of Pt/WS_2 (0.88 wt% Pt loading) with higher costs. Characteristic results indicate that WO_3 impurities were in-situ produced on the WS_2 surface and the Pd NPs are primarily located inside the WS_2 nanocages. Contrasting experiments suggest that the WO_3 impurities play a crucial role in generating H_{ads} intermediate and the Pd NPs are active sites of H_2 production, and a reaction mechanism is proposed. The Pd/WS_2 catalyst also shows good long-term stability owing to the location of Pd NPs inside the WS_2 cages. The high HER activity, low costs and good stability make the Pd catalyst a potential alternative to Pt catalyst for HER.

1. Introduction

The depletion of fossil fuels and the negative impact of environmental pollution promote the rapid development and use of renewable and sustainable alternative energy sources. As an important and highly promising energy source, hydrogen has been the focus of intensive research because of its renewability, abundant resources and zero pollution, meeting the future energy demands [1–3]. One of the most efficient routes to produce hydrogen is by hydrogen evolution reaction (HER) from water [4], which however requires high-performance HER electrocatalysts [5–7].

Platinum is a good HER electrocatalyst, but the scarcity and high costs hinder its wide commercial application [8,9], despite of the achievements made in recent years on e.g. preparing monolayer Pt catalyst [10], constructing hybrid structure with minimal Pt [11,12], and supporting Pt on large surface area substrates [13,14]. Low-cost transition metals were also tried for the aim of lowering the catalyst cost, but they encounter other problems such as low efficiency and poor stability [15]. Consequently, compromised metals such as palladium, which costs less than Pt [16] but shows higher activity and stability than transition metals, comes into the picture. For example, Barman et al. reported that porous palladium nanoparticles-carbon nitride composites exhibited high activity and durability towards HER in both acidic and alkaline media [17]. A recent review [48] has also underlined the promising prospect of applying Pd catalysts for HER.

Earth-abundant transition metal dichalcogenides are recognized as promising HER electrocatalysts [18–20]. WS_2 is an active electrocatalyst, and density functional theory (DFT) calculations suggest that it is comparable to the Pt-group metal for HER with respect to the free energy of hydrogen adsorption (ΔG_{H^*}) on the WS_2 edges [21]. Hence, WS_2 is usually fabricated in nano forms [22–25], rather than bulk [26,27], when used as catalyst for HER,

* Corresponding author at: Hubei Key Laboratory of Biomass Fibers and Eco-dyeing & Finishing, College of Chemistry and Chemical Engineering, Wuhan Textile University, Wuhan 430200, PR China.
E-mail address: jjzhu@wtu.edu.cn (J. Zhu).
[1] Both authors contributed equally to this work.

https://doi.org/10.1016/j.jcat.2019.10.007
0021-9517/

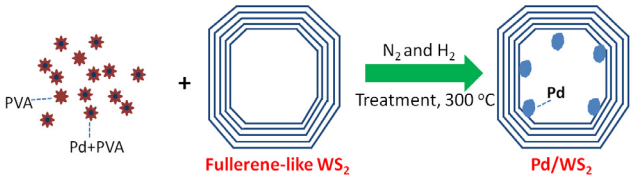

Scheme 1. Sketch map of the loading of Pd NPs to WS_2 cages.

in order to expose more surface edges. Nevertheless, the activity of WS_2 alone is not satisfactory as compared to that of Pt-based catalyst despite of the varied nanostructures designed, due to the limitation of intrinsic electronic structure, e.g., electrical conductivity. For this, hybridization with foreign species to tune the local electronic structure of WS_2 is suggested [28]. One interesting case is the hybridization of WO_3 to WS_2, namely, WO_3/WS_2, which showed noticeably enhanced HER activity compared to the respective WO_3 and WS_2 [29]. This is explained by the synergistic effects originated from WO_3 and WS_2, which result in not only increased active sites to produce hydrogen, but also enhanced conductivity to transfer electrons.

In this work, we report the use of inorganic fullerene-like (IF) WS_2 as support of Pd catalyst (Pd/WS_2) for HER conducted in acidic conditions. IF WS_2 has a cage structure like carbon fullerene, [30,31] and finds applications in many fields, such as nanoparticulate solid lubricants [32] and shock absorbers [33]. It has been reported that the analogue MoS_2 fullerene is active and shows improved activity for HER relative to the few-layer MoS_2, because of its enhanced density of edge sites. [34,35] We therefore believe that IF WS_2 can also exhibit exciting properties for HER, as it not only has large exposed surface edges but also offers the possibility to accommodate active metals inside the cages, improving the catalyst stability, as depicted in Scheme 1. Indeed, we found that the Pd NPs were mostly inside the WS_2 cages when prepared by the sol immobilization method [36]. In particular, WO_3 impurities were in-situ produced on the surface of WS_2 after loading the Pd NPs, due to the reaction between WS_2 and polyvinyl alcohol (PVA), which is a protecting agent of Pd NPs used in the preparation process. Consequently, cooperative effect between WO_3 and Pd NPs is induced, which enables the Pd/WS_2 catalyst exhibiting not only excellent activity but also good stability for HER.

2. Experimental section

2.1. Preparation of Pd/WS_2 and Pt/WS_2

The sample was prepared by sol-immobilization method as follows: 850 μL 22.1 mmol L^{-1} $PdCl_2$ and 500 μL 2 wt% polyvinyl alcohol (PVA) were first added to 150 mL H_2O, to which 870 μL 0.1 mol L^{-1} $NaBH_4$ was dropped stepwise. Then, 0.2 g quasi-spherical IF WS_2 nanoparticles (from Nanomaterials Ltd., Israel) were added to the mixture to immobilize the Pd sols on IF WS_2 under stirring, till the solution became colourless. The resulting material was then filtered, washed with distilled water 3 times and dried at 100 °C overnight, and finally treated at 350 °C in N_2 for 3 h and in H_2 for another 3 h under atmospheric pressure. The obtained sample was denoted as Pd/WS_2.

To change the Pd loading, different amounts of $PdCl_2$ solution were added with otherwise identical conditions. By this way, Pd/WS_2 catalysts with nominal Pd loading of 0.5 wt%, 1 wt%, and 1.5 wt% were prepared.

For comparison, four extra samples were prepared. Namely, Pd/CNT prepared using carbon nanotubes (CNT) as support, Pd/WO_3 prepared using WO_3 as support, Pd/WS_2-WI prepared without the addition of PVA, and Pt/WS_2 prepared using H_2PtCl_6 as precursor. Pt/C (20 wt% Pt on Vulcan XC-72R) as reference material was purchased from Sigma-Aldrich Chemical Reagent Co., Ltd.

2.2. Catalyst characterizations

Powder X-ray diffraction (XRD) patterns were measured on a Rigaku Ultima IV X-ray instrument using Kα radiation (λ = 1.5418 Å). N_2 adsorption-desorption isotherms were measured on a TriStar II 3020 physisorption apparatus at −196 °C and the surface areas were calculated by multiple points using the Brunauer-Emmett-Teller (BET) method based on the adsorption branch. Before measurements, the samples were treated in vacuum at 150 °C for 5 h. X-ray photoelectron spectroscopy (XPS) measurements were recorded on an ESCALAB 250Xi apparatus (Thermo Scientific) equipped with a monochromated Al Kα X-ray source. The binding energies were calibrated using C 1s at binding energy of 284.8 eV. Transmission electron microscopy (TEM) analysis of the samples was done on a FEI Tecnai G^2 S-Twin instrument equipped with a field emission gun operating at 200 kV. The powder was ultrasonically dispersed in ethanol for several seconds before being deposited on the carbon coated copper grid for observation. Scanning electron microscopy (SEM) and energy-dispersive X-ray spectroscopy (EDS), performed on Hitachi SU8010 equipment, were used for elemental analysis of the Pd/WS_2 catalyst. The metal loadings were determined on an Agilent 7900 inductively coupled plasma mass spectrometer (ICP-MS). The sample (50 mg) was added to 20 mL HCl and HNO_3 solution (1:1 in volume), sealed in autoclave and heated at 100 °C for 6 h. After cooling down to room temperature, the resulting solution was diluted with deionized water to 50 mL for analysis.

2.3. Electrocatalytic reaction

Electrocatalytic tests were conducted on a CHI 660E (Chenhua, Shanghai) electrochemistry workstation with standard three-electrode cell. Saturated calomel electrode (SCE) and platinum wire were used as the reference and the counter electrode, respectively. A glassy carbon (GC) electrode loaded with catalyst was used as the working electrode, which was prepared as follows: 3 mg catalyst was dispersed in 200 μL isopropanol and sonicated for 30 min, then 3 μL of the resulting ink was dropped onto the GC electrode, and 2 μL 0.3 wt% Nafion-isopropanol solution was dropped on top of the dried film, yielding a catalyst concentration of ca. 0.43 mg cm^{-2}.

Polarization curves were obtained by linear sweep voltammetry at a scan rate of 5 mV s^{-1} in 0.5 M H_2SO_4. The durability of catalyst was assessed by accelerated linear potential sweeps conducted repeatedly at a scan rate of 5 mV s^{-1}. The reaction was done by inserting the electrodes directly to the solution without purging inert gas (e.g., N_2) to remove any dissolved gases, as no appreciable difference in the HER activity was observed when N_2 was purged for one hour before the tests (see Fig. S1). Electrochemical impedance spectroscopy (EIS) was carried out at η = 0.1 V from 10^{-1} to 10^6 Hz with an AC voltage amplitude of 5 mV. The potentials (E), measured against the SCE electrode, were converted to the reversible hydrogen electrode (RHE) scale, according to equation $E_{(versus\ RHE)} = E_{(versus\ SCE)} + E_{0\ (SCE)} + 0.059pH$.

3. Results and discussion

Fig. 1A displays the XRD pattern of the catalysts. The bare WS_2 shows diffraction peaks at 14.3°, 32.8°, 39.3°, 43.9° and 58.4° that are respectively assigned to the (0 0 2), (1 0 0), (1 0 3), (0 0 6) and (1 1 0) lattice planes of hexagonal structure of WS_2 (JCPDS No.

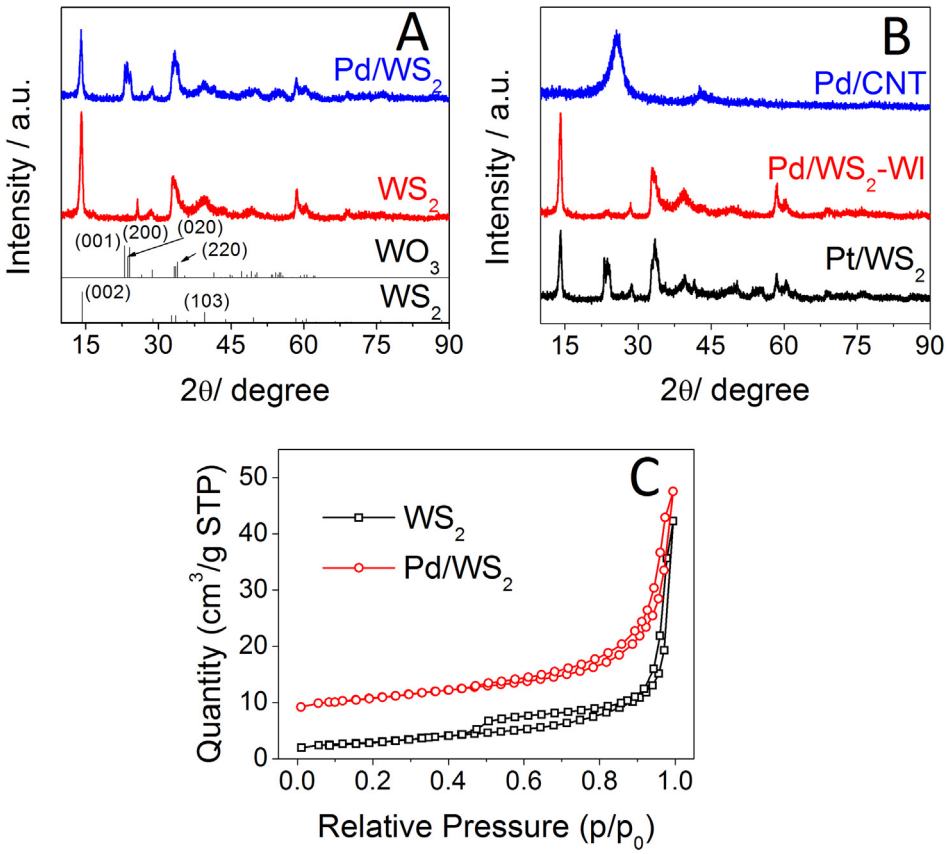

Fig. 1. The XRD patterns (A–B) and the N_2-physisorption isotherms (C) of the bare WS_2, Pd/WS_2, Pt/WS_2, Pd/WS_2-WI and Pd/CNT samples. (Note: the N_2-physisorption isotherms of Pd/WS_2 was up-shifted to differentiate the two curves).

08-0237). After the deposition of Pd NPs, some new diffraction peaks at 24.0° and 33.5° that are assigned to WO_3 (JCPDS No. 20-1324) appear, indicating that a low amount of WS_2 was in-situ converted into WO_3. Since no oxygen was present in the heat-treatment process, we consider that the oxidation of WS_2 to WO_3 is due to the presence of PVA, which contains oxygen atoms. That is, WO_3 is formed from the reaction of WS_2 and PVA during the heat-treatment step. To support this, a contrasting sample Pd/WS_2-WI was prepared without adding PVA, which shows no diffraction peak assigned to WO_3 (Fig. 1B), confirming our assumptions. It is worth noting that no diffraction peak assignable to Pd or Pt appears for all the samples (Fig. 1A–B), this suggests that the Pd or Pt NPs are finely dispersed on the supports. The crystalline size of WS_2 calculated by the Scherrer equation using the diffraction peak at $2\theta = 14°$, is 14.4 and 15.7 nm for Pd/WS_2 and Pd/WS_2-WI, respectively, indicating that the impregnation of Pd and Pt does not influence much on the WS_2 structure.

Fig. 1C displays the N_2-physisorption isotherms of WS_2 and Pd/WS_2, with the textural data listed in Table 1 and pore size distribution presented in Fig. S2A. Comparing to that of the bare WS_2, the BET surface area of Pd/WS_2 increases by ~40%, while the pore size decreases by ~30%. This is likely the result of the Pd NPs being located inside the WS_2 cages, which provides more surfaces to absorb N_2 and meanwhile decreases the actual space within the WS_2 cages (i.e., smaller average pore size). Similar trend is also observed for Pt/WS_2, as depicted in Fig. S2B of the SI.

ICP-MS analysis confirms the loading of Pd and Pt NPs on WS_2, with Pd loading of 0.76 wt% for Pd/WS_2 and Pt loading of 0.88 wt% for Pt/WS_2.

Fig. 2 shows TEM images of the pristine WS_2 and Pd/WS_2 with different magnifications. For WS_2, individual semi-spherical nanoparticles are revealed and a multi-layered, closed-cage structure with average diameter of 80 nm is observed, in accordance to that reported in previous works [50,51]. The high-resolution TEM image depicts a lattice spacing of 0.62 nm, corresponding to the (0 0 2) plane of WS_2, Fig. 2C. For Pd/WS_2, both the structure and the exposed lattice planes (0 0 2) of WS_2 were seemingly not destroyed after the Pd loading. Meanwhile, a new lattice spacing of 0.39 nm, corresponding to the (0 0 1) planes of WO_3, is observed on the shells of WS_2, suggesting that part of the WS_2 were converted into WO_3.

As for the Pd NPs, they are homogeneously dispersed on the surface of WS_2, with average diameter of ca. 10 nm. The contrast of Pd NPs to WS_2 is low, which suggests that the Pd NPs are underneath the WS_2 surface. EDS mappings obtained from SEM measurements (Fig. 2G–K) show that a certain amount of Pd exists, and it is homogeneously dispersed in WS_2. It is worth noting that oxygen atoms are also detected, and their density is higher than that of palladium atoms. This could be due to the formation of WO_3 species and a higher mole amount of WO_3 than that of Pd. TEM images of Pt/WS_2 show also the WS_2 fullerene-like structure and the WO_3 (0 0 1) lattice plane, Fig. S3, like that of Pd/WS_2.

Table 1
The textural properties and Pd loading obtained for WS_2 and Pd/WS_2.

Sample	$S_{BET}/m^2\ g^{-1}$	P. V./$cm^3\ g^{-1}$[a]	P. S./nm[b]	Pd loading/%[c]
WS_2	10.5	0.065	21.6 (2.6)[d]	–
Pd/WS_2	14.5	0.063	15.5 (2.6)[d]	0.76

[a] Pore volume obtained by N_2 physisorption isotherms.
[b] Pore size obtained by N_2 physisorption isotherms.
[c] Pd loading determined from ICP-MS.
[d] The value in the bracket is the size of the WS_2 cages.

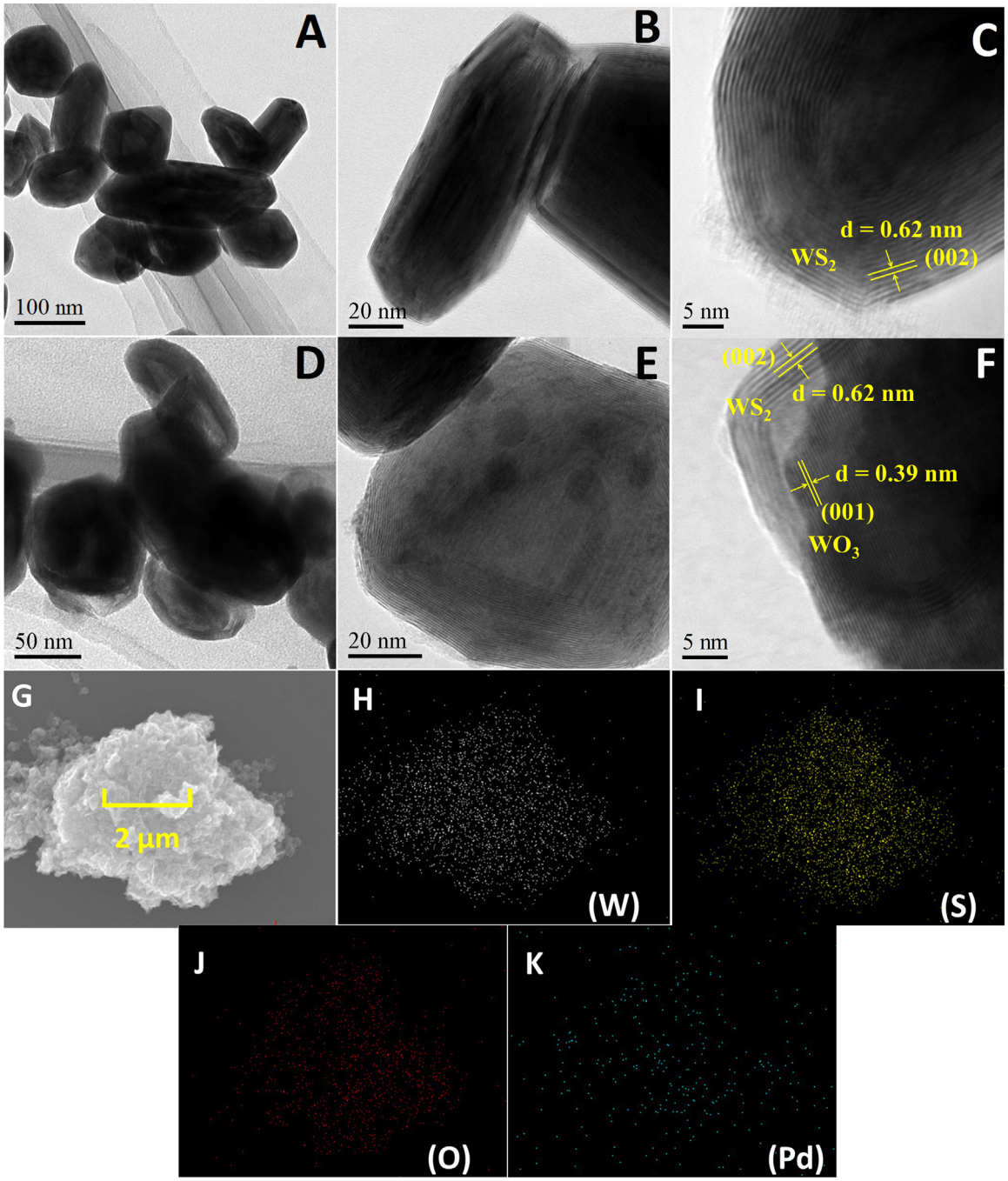

Fig. 2. TEM images of the bare WS_2 NPs (A–C) and the Pd/WS_2 catalyst (D–F); EDS mapping of Pd/WS_2 measured by SEM measurements (G–K).

Identification of the actual location of Pd NPs, inside or outside of the WS_2 cages, by EDS mappings of either SEM or TEM is not feasible, since the Pd NPs are dispersed homogeneously in WS_2, which is unlike that of core-shell material. Hence, we did not make effort to prove the actual location of Pd NPs by EDS mappings.

It is known that where the molecular layers of these nested fullerene-like structure fold, often a kink is formed leaving a void [37]. Previous analysis by XRD demonstrated that the experimental diffraction intensities from the WS_2 NPs are substantially distorted compared to bulk material, and line shapes and intensities were found to be consistent with a random stacking of trigonal prismatic layers rather than a mixture of hexagonal and rhombohedral bulk phase. The prismatic (hk0) faces are chemically reactive due to the abundance of dangling bonds and therefore are more prone to a chemical degradation by an oxidation process [38]. In our study, oxidation (specifically, the formation of WO_3 impurities) was observed when oxygen containing PVA was present in the heat-treatment process.

Fig. 3 shows the XPS spectra of WS_2 and Pd/WS_2. For WS_2, the three peaks centered at 32.6, 34.7 and 38.4 eV are characteristic peaks of W^{4+} species associated to W $4f_{7/2}$, W $4f_{5/2}$ and W $5p_{3/2}$, respectively (Fig. 3A) [39], and the two peaks at 162.2 and 163.4 eV are characteristic peaks of S^{2-} species associated to S $2p_{1/2}$ and S $2p_{3/2}$, respectively (Fig. 3B) [29]. Two rather weak peaks centered at 36.0 and 38.0 eV were also deconvolved, which might indicate the presence of W^{6+} species (e.g., the oxidation of WS_2 to WO_3 by the oxygen present in the air). However, the one strong peak centered at 532.0 eV with Gaussian distribution (Fig. 3C)

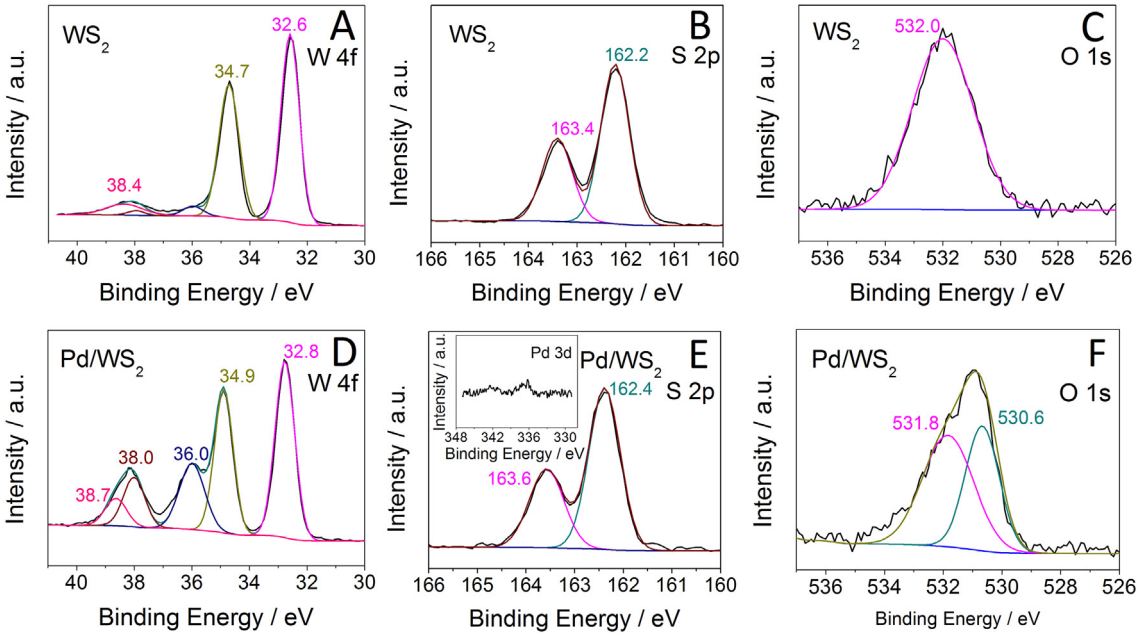

Fig. 3. The fine W 4f, S 2p and O 1s XPS spectra of the bare WS_2 (A–C) and the Pd/WS_2 catalyst (D–F), respectively. The inset in E shows the Pd 3d XPS spectrum of Pd/WS_2.

Table 2
Surface elemental analyses of WS_2 and Pd/WS_2, based on the data obtained from the XPS spectra.

Sample	Surface atomic percentage/%				S/W[a]
	O 1s	W 4f	S 2p	Pd 3d	
WS_2	16.7	21.2	50.6	–	2.4
Pd/WS_2	32.4	19.9	32.5	1.4	1.6

[a] Surface atomic ratio of S to W from XPS spectra.

suggests that no lattice oxygen is present and this peak is most likely assigned to the binding energy of oxygen that was chemically adsorbed on the surface, e.g. O_2 and/or H_2O [29,51]. Thus, we assume that the peaks at 36.0 and 38.0 eV do not imply that WO_3 is formed on the surface, but that a small amount of W^{4+} species was surrounded by the adsorbed oxygen, leading to the presence of fake W^{6+} species (e.g., $[W^{4+}\text{-}O_2] \rightarrow [W^{6+}\text{-}O_2^{2-}]$).

For Pd/WS_2, besides those associated to the W^{4+} species, the peaks centered at 36.0 and 38.0 eV, attributed respectively to the W $4f_{7/2}$ and W $4f_{5/2}$ of W^{6+} species of WO_3 [29], are detected with well-resolved peak intensity (Fig. 3D). This suggests that some surface W^{4+} species (WS_2) are converted to W^{6+} species (WO_3) after the Pd loading, supporting the observations from XRD and TEM measurements. This is also confirmed from the change of the O 1s spectrum, Fig. 3F, in which a new peak centered at 530.6 eV, assigned to O^{2-} species of WO_3 [53], appears, and that the surface atomic percentage of O 1s increases from 16.7% for WS_2 to 32.4% for Pd/WS_2. No obvious difference in the S 2p XPS spectra is observed between Pd/WS_2 and WS_2, indicating that the sulfur exists as S^{2-} species and no sulfate forms. However, from the atomic ratio of S/W, we see that the ratio decreases obviously from 2.4 for WS_2 to 1.6 for Pd/WS_2 (Table 2), suggesting the formation of surface S defects and WO_3. Possibly, some sulfur atoms were also converted to SO_2 or H_2S by reacting with PVA during the Pd/WS_2 formation process.

The signal of the Pd 3d XPS spectrum is extremely low (see the insert picture in Fig. 3E), which implies that only low amounts of Pd NPs are detected and exposed on the WS_2 surface. Considering the Pd loading of 0.76 wt%, which is enough to conduct XPS measurements with good signal quality, we infer that most of the Pd NPs are not located on the external surface, but inside the WS_2 cages, as supported by the change in the average pore size, which decreases from 21.6 nm for WS_2 to 15.5 nm for Pd/WS_2, Table 1. Even for the Pt/WS_2 catalyst, with a Pt loading of 0.88 wt%, it shows an extremely low signal in the Pt 4f XPS spectrum, Fig. S4. This suggests again that the Pd or Pt NPs are likely formed inside the WS_2 cages.

Fig. 4A demonstrates the polarization curves (I-V plot) of the various catalysts, showing that Pd/WS_2 has an onset overpotential (η) of ~47 mV, and the overpotential at 10 mA/cm^{-2} current density, which is a typical reference to evaluate the electrocatalytic performance, is 130 mV. The small η value indicates that the Pd/WS_2 can be a promising catalyst for H_2 production by HER route. The exchange current density (J_0) was calculated to be 0.264 mA cm^{-2}. The I-V plot of Pd/WS_2 was also made by normalizing the electrochemical surface area (ECSA), as shown in Fig. S5. Besides, it is worth noting that the Pd loading was set at 1 wt% in this work, since it shows abrupt improvement in the HER activity as compared to 0.5 wt% Pd, while comparable HER activity to 1.5 wt% Pd, Fig. S6.

In contrast, the bare WS_2 shows extremely poor HER activity, with the η value exceeding 550 mV. This suggests that the activity of Pd/WS_2 is mostly contributed by the Pd NPs and the WS_2 acts merely as a support. However, a very poor HER activity is also observed for Pd/CNT, which indicates that the HER activity depends not solely on the Pd NPs. This is further supported by the Tafel slope obtained based on the equation: $\eta = a + b * \log|j|$, using the data in Fig. 4A, where the constant "b" represents the Tafel slope and is calculated from the slope of the above function. Fig. 4B shows the Tafel slope of Pd/WS_2 is 82.4 mV dec^{-1}, which is lower than that of bare WS_2 (124.3 mV dec^{-1}) and Pd/CNT (112.4 mV dec^{-1}). It is thus inferred that a synergistic effect must be induced in the Pd/WS_2 catalyst, which accounts for the good HER activity.

To support the assumption that a synergistic effect was induced in the presence of WO_3 impurities, two contrasting experiments were conducted. First, we tested the catalytic performances of a

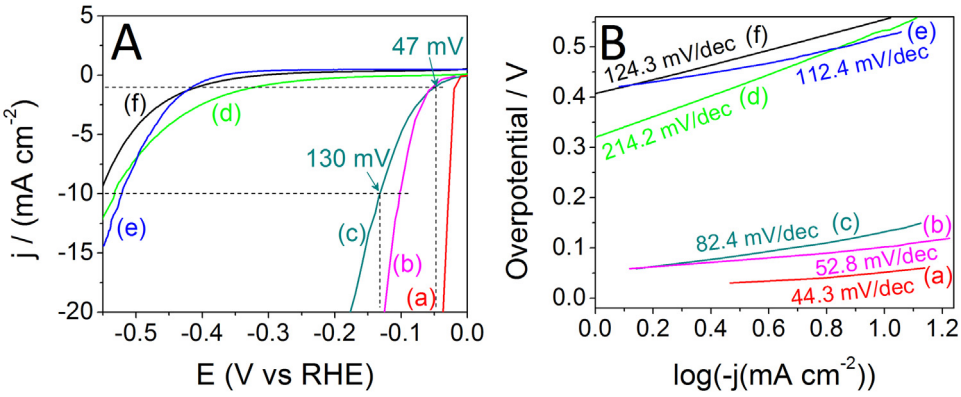

Fig. 4. HER polarization curves (A) and the corresponding Tafel slopes (B) of the investigated samples. (a) Pt/C, (b) Pt/WS_2, (c) Pd/WS_2, (d) Pd/WS_2-WI, (e) Pd/CNT and (f) WS_2.

WO_3-free Pd/WS_2-WI catalyst, which showed very poor HER activity (curve *d* of Fig. 4), suggesting that the absence of WO_3 impurities deactivates the catalyst. Second, we tested and compared the activity of WS_2, WO_3, Pd/WO_3 and Pd/WS_2 (see Fig. S7), finding that although the pure WO_3 shows far better activity than the pure WS_2, Pd/WO_3 exhibited lower activity than Pd/WS_2 that contains a few amount of WO_3 impurities, indicating that the presence of WO_3 impurities can promote significantly the activity of Pd/WS_2. These results confirm that the presence of WO_3 impurities is crucial for the reaction and a synergistic effect between WO_3 and WS_2 is induced in Pd/WS_2.

The role of WO_3 impurities in the reaction can be that it provides a route for the transformation of H^+ ions to molecular H_2 or adsorbed H_{ads}, by forming H_xWO_3 intermediate [30,40,41], as described by reactions (1) and (2):

$$xH^+ + xe^- + WO_3 \rightarrow H_xWO_3 \quad (1)$$

$$2H_xWO_3 \rightarrow xH_2 + 2WO_3 \quad (2)$$

where x is a stoichiometric parameter and varies from 0 to 1. The active H atoms of H_xWO_3 can also diffuse to the nearby Pd or WS_2 NPs and adsorb on their surface, by reactions (3) and (4) [30,52]:

$$H_xWO_3 + Pd \rightarrow xH_{ads}\text{-}Pd + WO_3 \quad (3)$$

$$H_xWO_3 + WS_2 \rightarrow xH_{ads}\text{-}WS_2 + WO_3 \quad (4)$$

where H_{ads} represents the H atom adsorbed at an active site.

Besides the WO_3 impurities, the sulfur deficiency may also play an important role in the reaction. As observed in Table 2, the molar ratio of S/W decreases significantly after the deposition of Pd NPs, which indicates the formation of sulfur deficiency. These deficiencies can act as the adsorption sites of H atoms and promote the production of H_2 molecules, improving the HER activity, in accordance to that observed in previous literature [42–44].

According to the classical theory in acidic electrolyte, two mechanisms can be applied for HER, described as Volmer-Heyrovsky and Volmer-Tafel reactions (5)–(7) [45,46]:

$$\text{Volmer reaction: } H_3O^+ + e^- \rightarrow H_{ads} + H_2O \quad (5)$$

$$\text{Heyrovsky reaction: } H_{ads} + H_3O^+ + e^- \rightarrow H_2 + H_2O \quad (6)$$

$$\text{Tafel reaction: } H_{ads} + H_{ads} \rightarrow H_2 \quad (7)$$

The rate-limiting step of HER has a close relation to the Tafel slope [46]. Generally, it is considered that the Tafel slope of 40–120 mV dec^{-1} is the threshold to judge the rate-limiting step. For reaction with Tafel slope above 120 mV dec^{-1} the rate-limiting step is determined by the Volmer reaction, and below 40 mV dec^{-1} it is determined by the Tafel reaction, while at intermediate values 40–120 mV dec^{-1} it is determined by the Heyrovsky reaction. It is known that the HER on Pt/C catalyst with Tafel slope of 30 mV dec^{-1} follows the Volmer-Tafel route [45].

Based on the Tafel slopes of WS_2 and Pd/WS_2 shown in Fig. 4B, it is inferred that the rate-limiting step of HER changes from Volmer reaction for WS_2 to Heyrovsky reaction for Pd/WS_2. That is, the production of H_{ads} species is facilitated after the deposition of Pd NPs on WS_2. This is reasonable as WO_3 impurities are generated in Pd/WS_2, which provide additional route to produce H_{ads}, by reactions (3) and (4), increasing the rate of H_{ads} production. Therefore, we consider that the crucial step of reaction (6) is that the H_3O^+ species cannot be supplied efficiently enough, limiting the overall reaction by local depletion. The importance of supplying H^+ to the reaction is verified by the results that both Pd/WS_2 and WS_2, show poor HER activity when conducted in neutral conditions, Fig. S8. Barman et al. also reported that the HER activity of Pd catalysts depends intimately on the solution pH, and that when conducted at higher pH values exhibit lower HER activity, supporting our findings [17].

Accordingly, a new mechanism for HER conducted on Pd/WS_2 is proposed based on the role of WO_3 impurities, Fig. 5. We suppose that the Pd NPs are located inside the WS_2 cages, and the WO_3 impurities, formed from the reaction of WS_2 and PVA, exist both on the external and internal surfaces of WS_2 cages, since the PVA

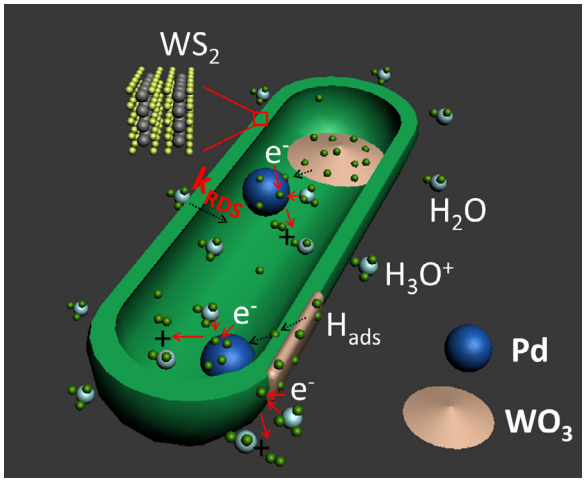

Fig. 5. Proposed mechanism for HER conducted on Pd/WS_2 in acidic conditions.

in solution can diffuse anywhere and reaction can thus take place at the defects within the WS_2 or at the outermost layer. During the HER tests, the H_{ads} species can be produced by reactions (3) and (4) through the formation of H_xWO_3 intermediate, reaction (1). Along with reaction (5), the H_{ads} species can thus be facilely produced. However, this would lead to the fast consumption of H^+ ions, especially those inside the WS_2 cages, making the local supply of H_3O^+ to reaction (6) problematic. In order to enable the reaction (6) to occur, the H_3O^+ species in solution need to penetrate the pores of WS_2. This takes some time and the Heyrovsky reaction becomes the rate-limiting step. This also implies that the HER occurs mainly inside the WS_2 cages, and that the Pd NPs are the active sites of reaction.

For comparison, the HER activities of Pt/WS_2 were also measured and are presented in Fig. 4, showing an η value of 100 mV and a Tafel slope of 52.8 mV dec^{-1}, which is better than that obtained from Pd/WS_2, and suggests that Pt is better than Pd for HER. However, the Pt loading measured by ICP-MS is 0.88 wt%, which is higher than that of Pd (0.76 wt%). Therefore, when considering the metal loading, the difference in the HER activities of Pd/WS_2 and Pt/WS_2 becomes only marginal. In addition, we found that the commercial Pt/C (20 wt%, Sigma-Aldrich Chemical Reagent Co., Ltd.), which is a frequently used standard HER catalyst, exhibits an η value of 30 mV and a Tafel slope of 44.3 mV/dec, which is certainly better than that of Pd/WS_2 and Pt/WS_2, but its Pt loading is 23 times higher than that of Pd/WS_2 or Pt/WS_2. Hence, even compared to the commercial Pt/C (20 wt% Pt loading-), the Pd/WS_2 electrocatalyst prepared in this study has certain superiorities if the metal loading, and especially the metal costs, are considered.

Li et al. reported that the HER activities of Pd/Mo_2C depend intimately on the Pd loading (3–12 wt%), with the lowest Pd loading (3 wt%) showing the lowest activity and an η value of 135 mV [47]. The Pd/WS_2 prepared in this work with much lower Pd loading (0.76 wt%) shows comparable electrocatalytic activity (η value of 130 mV) to that of Pd/Mo_2C (3 wt%), for example, indicating that it is possible to lower the Pd loading (or catalyst cost) while achieving comparable activity. It is expected that higher HER activity could be achieved when increasing the Pd loading of Pd/WS_2. A comparison to other Pd or Pt based catalysts also demonstrates that the Pd/WS_2 catalyst in our work has comparable activity for HER (see Table S1), especially if the catalyst cost is considered.

Finally, electrochemical impedance spectroscopy (EIS) of Pd/WS_2 and Pt/WS_2 was conducted to illuminate the natural difference between them and relate to their catalytic behaviors, Fig. 6A. It shows that the solution resistance (R_s) of Pd/WS_2 and Pt/WS_2 is similar, with a value of 8 and 11 Ω, respectively. This indicates that the source resistance of both catalysts is close, and the activity difference caused by the electrode fabrication process can be neglected. On the other hand, the charge transfer resistance (R_{ct}) that is reflected by the diameter of the semicircle, exhibits a larger value for Pd/WS_2 (ca. 90 Ω) than for Pt/WS_2 (ca. 60 Ω). This means that the electron transfer at the electrode-electrolyte interface is slower on Pd/WS_2 than that on Pt/WS_2, or the H^+ reduction is more difficult when Pd/WS_2 is used as the electrode. The reason could be attributed to the better electronic conductivity of Pt (vs. Pd) and its higher loadings (0.88 wt% for Pt/WS_2 and 0.76 wt% for Pd/WS_2). Therefore, the lower HER activity of Pd/WS_2 is not attributed to the external factor (e.g., the contact between the electrode and the catalyst), but to the intrinsic properties of Pd/WS_2.

Nevertheless, the Pd/WS_2 has good long-term HER stability and is comparable to that of Pt/WS_2, with no appreciable loss in the activity after 1000 cycles, Fig. 6B–C, indicating that Pd/WS_2 could meet the standard of commercial catalyst with respect to reusability. For comparison, the stability of a referenced Pt/C catalyst was

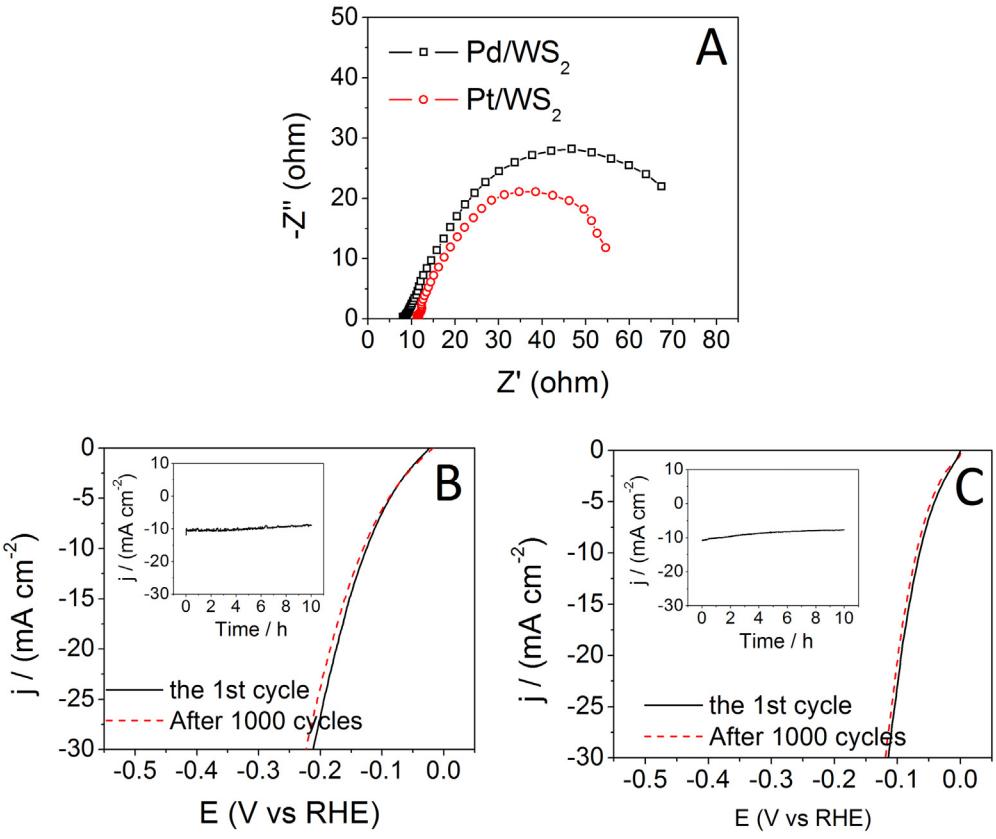

Fig. 6. Nyquist plots of Pd/WS_2 and Pt/WS_2 acquired by EIS measurements (A); HER polarization curves of Pd/WS_2 (B) and Pt/WS_2 (C) before and after 1000 cycles conducted in 0.5 M H_2SO_4 solution. The insets show cathodic current densities as a function of time up to 10 h duration. The potential range for the cycling experiments is 0 to −0.558 V.

also tested, and the result is presented in Fig. S9. (Note that because many bubbles were produced on the electrode's surface, making the polarization curves hard to measure, we plotted a time-dependent curve instead for this sample). Therefore, we believe that Pd/WS_2 could be a promising alternative to Pt catalyst for HER for industrial use, if the metal loading and catalyst costs are considered. A challenging technology is to regulate the synergistic effect between Pd and WS_2 to decrease the charge transfer impedance, which will be our future research directions.

4. Conclusions

Inorganic fullerene-like WS_2 supported Pd catalysts (Pd/WS_2) were synthesized by the sol immobilization method and their catalytic performances for hydrogen evolution reaction (HER) from water were investigated. The Pd nanoparticles (NPs) were seemingly formed inside the WS_2 cages and a small amount of surface WS_2 was oxidized to WO_3 by reacting with the protecting agent (i.e., PVA) of the Pd NPs. The Pd/WS_2 electrocatalyst was highly active for HER with comparable performance to the Pt based catalyst. The presence of WO_3 species, which provide an additional route to produce adsorbed hydrogen (H_{ads}) was found to be at the origin of the high HER activity. In reaction conditions of 0.5 M H_2SO_4 solution, the Tafel slope of Pd/WS_2 for HER was 82.4 mV dec^{-1} and the reaction obeyed Volmer-Heyrovsky mechanism. This suggests that the supply of H_3O^+ species, from solution to the WS_2 cages, is crucial to the reaction, and that the HER occurred mainly inside the WS_2 cages, where the Pd NPs active sites are located. Because of the confinement of Pd NPs in the WS_2 cages, the Pd/WS_2 catalyst shows good long-term stability for HER, with no appreciable loss of activity observable after running for 1000 cycles. The efficient and stable HER activity, together with the low costs, make the Pd/WS_2 catalyst promising for HER in future.

Declaration of Competing Interest

The authors declare that they have no known competing financial interests or personal relationships that could have appeared to influence the work reported in this paper.

Acknowledgements

This work was supported by the National Natural Science Foundation of China (21976141, 21601128, 21761162016), the Key Research and Development Program of MOST (2017YFE0131200) and the Central Committee Guides Local Science and Technology Development Special Project of Hubei Province (2019ZYYD073).

Appendix A. Supplementary material

Supplementary data to this article can be found online at https://doi.org/10.1016/j.jcat.2019.10.007.

References

[1] M.S. Dresselhaus, I.L. Thomas, Alternative energy technologies, Nature 414 (2001) 332–337.
[2] J.A. Turner, Sustainable hydrogen production, Science 305 (2004) 972–974.
[3] J. Qi, W. Zhang, R. Cao, Solar-to-hydrogen energy conversion based on water splitting, Adv. Energy Mater. 8 (2017) 1701620.
[4] M.G. Walter, E.L. Warren, J.R. McKone, S.W. Boettcher, Q. Mi, E.A. Santori, N.S. Lewis, Solar water splitting cells, Chem. Rev. 110 (2010) 6446–6473.
[5] N.S. Lewis, D.G. Nocera, Powering the planet: chemical challenges in solar energy utilization, Proc. Natl. Acad. Sci. 103 (2006) 15729.
[6] A. Phuruangrat, D.J. Ham, S. Thongtem, J.S. Lee, Electrochemical hydrogen evolution over MoO_3 nanowires produced by microwave-assisted hydrothermal reaction, Electrochem. Commun. 11 (2009) 1740–1743.
[7] X. Wang, Y.V. Kolen'ko, X.Q. Bao, K. Kovnir, L. Liu, One-step synthesis of self-supported nickel phosphide nanosheet array cathodes for efficient electrocatalytic hydrogen generation, Angew. Chem. Int. Ed. 54 (2015) 8188–8192.
[8] C. Wang, F. Hu, H. Yang, Y. Zhang, H. Lu, Q. Wang, 1.82 wt.% Pt/N, P co-doped carbon overwhelms 20 wt.% Pt/C as a high-efficiency electrocatalyst for hydrogen evolution reaction, Nano Res. 10 (2017) 238–246.
[9] I.E.L. Stephens, I. Chorkendorff, Minimizing the use of platinum in hydrogen-evolving electrodes, Angew. Chem. Int. Ed. 50 (2011) 1476–1477.
[10] D.V. Esposito, S.T. Hunt, A.L. Stottlemyer, K.D. Dobson, B.E. McCandless, R.W. Birkmire, J.G. Chen, Low-cost hydrogen-evolution catalysts based on monolayer platinum on tungsten monocarbide substrates, Angew. Chem. Int. Ed. 49 (2010) 9859–9862.
[11] J.B. Raoof, R. Ojani, S.A. Esfeden, S.R. Nadimi, Fabrication of bimetallic Cu/Pt nanoparticles modified glassy carbon electrode and its catalytic activity toward hydrogen evolution reaction, Int. J. Hydrogen Energy 35 (2010) 3937–3944.
[12] C. Wang, K.E. deKrafft, W. Lin, Pt nanoparticles@photoactive metal-organic frameworks: efficient hydrogen evolution via synergistic photoexcitation and electron injection, J. Am. Chem. Soc. 134 (2012) 7211–7214.
[13] G.R. Xu, J.J. Hui, T. Huang, Y. Chen, J.M. Lee, Platinum nanocuboids supported on reduced graphene oxide as efficient electrocatalyst for the hydrogen evolution reaction, J. Power Sour. 285 (2015) 393–399.
[14] S. Bai, C. Wang, M. Deng, M. Gong, Y. Bai, J. Jiang, Y. Xiong, Surface polarization matters: enhancing the hydrogen-evolution reaction by shrinking Pt Shells in Pt–Pd–graphene stack structures, Angew. Chem. Int. Ed. 53 (2014) 12120–12124.
[15] W.F. Chen, J.T. Muckerman, E. Fujita, Recent developments in transition metal carbides and nitrides as hydrogen evolution electrocatalysts, Chem. Commun. 49 (2013) 8896–8909.
[16] M. He, Y. Ma, L. Yin, G. Cao, Q. Huang, W. Wei, H. Zhao, D. Zhang, M. Wang, T. Yang, Pt-Pd Bimetal Popcorn Nanocrystals: Enhancing the Catalytic Performance by Combination Effect of Stable Multipetals Nanostructure and Highly Accessible Active Sites, Small 14 (2018) 1703613.
[17] T. Bhowmik, M.K. Kundu, S. Barman, Palladium Nanoparticle–Graphitic Carbon Nitride Porous Synergistic Catalyst for Hydrogen Evolution/Oxidation Reactions over a Broad Range of pH and Correlation of Its Catalytic Activity with Measured Hydrogen Binding Energy, ACS Catal. 6 (2016) 1929–1941.
[18] D. Merki, X. Hu, Recent developments of molybdenum and tungsten sulfides as hydrogen evolution catalysts, Energy Environ. Sci. 4 (2011) 3878–3888.
[19] D.Y. Chung, S.K. Park, Y.H. Chung, S.H. Yu, D.H. Lim, N. Jung, H.C. Ham, H.Y. Park, Y. Piao, S.J. Yoo, Y.E. Sung, Edge-exposed MoS_2 nano-assembled structures as efficient electrocatalysts for hydrogen evolution reaction, Nanoscale 6 (2014) 2131–2136.
[20] L. Yang, W. Zhou, D. Hou, K. Zhou, G. Li, Z. Tang, L. Li, S. Chen, Porous metallic MoO_2-supported MoS_2 nanosheets for enhanced electrocatalytic activity in the hydrogen evolution reaction, Nanoscale 7 (2015) 5203–5208.
[21] T.F. Jaramillo, K.P. Jørgensen, J. Bonde, J.H. Nielsen, S. Horch, I. Chorkendorff, Identification of active edge sites for electrochemical H_2 evolution from MoS_2 nanocatalysts, Science 317 (2007) 100–102.
[22] Y. Zhang, J. Yan, X. Ren, L. Pang, H. Chen, S. Liu, 2D WS_2 nanosheet supported Pt nanoparticles for enhanced hydrogen evolution reaction, Int. J. Hydrogen Energy 42 (2017) 5472–5477.
[23] L. Cheng, W. Huang, Q. Gong, C. Liu, Z. Liu, Y. Li, H. Dai, Ultrathin WS_2 nanoflakes as a high-performance electrocatalyst for the hydrogen evolution reaction, Angew. Chem. Int. Ed. 53 (2014) 7860–7863.
[24] K. Xu, F. Wang, Z. Wang, X. Zhan, Q. Wang, Z. Cheng, M. Safdar, J. He, Component-controllable $WS_{2(1-x)}Se_{2x}$ nanotubes for efficient hydrogen evolution reaction, ACS Nano 8 (2014) 8468–8476.
[25] J. Lin, Z. Peng, G. Wang, D. Zakhidov, E. Larios, M.J. Yacaman, J.M. Tour, Enhanced electrocatalysis for hydrogen evolution reactions from WS_2 nanoribbons, Adv. Energy Mater. 4 (2014) 1301875.
[26] J. Yang, H.S. Shin, Recent advances in layered transition metal dichalcogenides for hydrogen evolution reaction, J. Mater. Chem. A 2 (2014) 5979–5985.
[27] A. Sobczynski, A. Yildiz, A.J. Bard, A. Campion, M.A. Fox, T. Mallouk, S.E. Webber, J.M. White, Tungsten disulfide: a novel hydrogen evolution catalyst for water decomposition, J Phys. Chem. 92 (1988) 2311–2315.
[28] J. Yang, D. Voiry, S.J. Ahn, D. Kang, A.Y. Kim, M. Chhowalla, H.S. Shin, Two-dimensional hybrid nanosheets of tungsten disulfide and reduced graphene oxide as catalysts for enhanced hydrogen evolution, Angew. Chem. Int. Ed. 52 (2013) 13751–13754.
[29] L. Yang, X. Zhu, S. Xiong, X. Wu, Y. Shan, P.K. Chu, Synergistic $WO_3{\cdot}2H_2O$ nanoplates/WS_2 hybrid catalysts for high-efficiency hydrogen evolution, ACS Appl. Mat. Interfaces 8 (2016) 13966–13972.
[30] R. Tenne, L. Margulis, M. Genut, G. Hodes, Polyhedral and cylindrical structures of tungsten disulphide, Nature 360 (1992) 444–446.
[31] L. Margulis, G. Salitra, R. Tenne, M. Talianker, Nested fullerene-like structures, Nature 365 (1993) 113–114.
[32] M. Chhowalla, G.A.J. Amaratunga, Thin films of fullerene-like MoS_2 nanoparticles with ultra-low friction and wear, Nature 407 (2000) 164–167.
[33] Y.Q. Zhu, T. Sekine, K.S. Brigatti, S. Firth, R. Tenne, R. Rosentsveig, H.W. Kroto, D.R.M. Walton, Shock-wave resistance of WS_2 nanotubes, J. Am. Chem. Soc. 125 (2003) 1329–1333.
[34] M. Chhetri, U. Gupta, L. Yadgarov, R. Rosentsveig, R. Tenne, C.N.R. Rao, Effects of p- and n-type doping in inorganic fullerene MoS_2 on the hydrogen evolution reaction, ChemElectroChem 3 (2016) 1937–1943.

[35] M. Chhetri, U. Gupta, L. Yadgarov, R. Rosentsveig, R. Tenne, C.N.R. Rao, Beneficial effect of Re doping on the electrochemical HER activity of MoS_2 fullerenes, Dalton Trans. 44 (2015) 16399–16404.
[36] Y. Önal, S. Schimpf, P. Claus, Structure sensitivity and kinetics of d-glucose oxidation to d-gluconic acid over carbon-supported gold catalysts, J. Catal. 223 (2004) 122–133.
[37] L. Houben, A.N. Enyashin, Y. Feldman, R. Rosentsveig, D.G. Stroppa, M. BarSadan, Diffraction from Disordered Stacking Sequences in MoS_2 and WS_2 Fullerenes and Nanotubes, J Phys. Chem. C 116 (2012) 24350–24357.
[38] B. Späth, F. Kopnov, H. Cohen, A. Zak, A. Moshkovich, L. Rapoport, W. Jägermann, R. Tenne, X-ray photoelectron spectroscopy and tribology studies of annealed fullerene-like WS_2 nanoparticles, Phys. Stat. Solidi B 245 (2008) 1779–1784.
[39] T.Y. Chen, Y.H. Chang, C.L. Hsu, K.H. Wei, C.Y. Chiang, L.J. Li, Comparative study on MoS_2 and WS_2 for electrocatalytic water splitting, Int. J. Hydrogen Energy 38 (2013) 12302–12309.
[40] X. Shang, Y. Rao, S.S. Lu, B. Dong, L.M. Zhang, X.H. Liu, X. Li, Y.R. Liu, Y.M. Chai, C.G. Liu, Novel WS_2/WO_3 heterostructured nanosheets as efficient electrocatalyst for hydrogen evolution reaction, Mater. Chem. Phys. 197 (2017) 123–128.
[41] B. Seo, H.Y. Jeong, S.Y. Hong, A. Zak, S.H. Joo, Impact of a conductive oxide core in tungsten sulfide-based nanostructures on the hydrogen evolution reaction, Chem. Commun. 51 (2015) 8334–8337.
[42] H. Li, C. Tsai, A.L. Koh, L. Cai, A.W. Contryman, A.H. Fragapane, J. Zhao, H.S. Han, H.C. Manoharan, F. Abild-Pedersen, J.K. Nørskov, X. Zheng, Activating and optimizing MoS_2 basal planes for hydrogen evolution through the formation of strained sulphur vacancies, Nat. Mater. 15 (2015) 48–53.
[43] A.Y. Lu, X. Yang, C.C. Tseng, S. Min, S.H. Lin, C.L. Hsu, H. Li, H. Idriss, J.L. Kuo, K. W. Huang, L.J. Li, High-sulfur-vacancy amorphous molybdenum sulfide as a high current electrocatalyst in hydrogen evolution, Small 12 (2016) 5530–5537.
[44] Y. Yin, J. Han, Y. Zhang, X. Zhang, P. Xu, Q. Yuan, L. Samad, X. Wang, Y. Wang, Z. Zhang, P. Zhang, X. Cao, B. Song, S. Jin, Contributions of phase, sulfur vacancies, and edges to the hydrogen evolution reaction catalytic activity of porous molybdenum disulfide nanosheets, J. Am. Chem. Soc. 138 (2016) 7965–7972.
[45] B.E. Conway, B.V. Tilak, Interfacial processes involving electrocatalytic evolution and oxidation of H_2, and the role of chemisorbed H, Electrochim. Acta 47 (2002) 3571–3594.
[46] X. Xiao, C. Engelbrekt, Z. Li, P. Si, Hydrogen evolution at nanoporous gold/tungsten sulfide composite film and its optimization, Electrochim. Acta 173 (2015) 393–398.
[47] T. Li, Z. Tang, K. Wang, W. Wu, S. Chen, C. Wang, Palladium nanoparticles grown on β-Mo_2C nanotubes as dual functional electrocatalysts for both oxygen reduction reaction and hydrogen evolution reaction, Int. J. Hydrogen Energy 43 (2018) 4932–4941.
[48] L. Zhang, Q. Chang, H. Chen, M. Shao, Recent advances in palladium-based electrocatalysts for fuel cell reactions and hydrogen evolution reaction, Nano Energy 29 (2016) 198–219.
[49] M. Shneider, H. Dodiuk, S. Kenig, R. Tenne, The Effect of Tungsten Sulfide Fullerene-Like Nanoparticles on the Toughness of Epoxy Adhesives, J. Adhes. Sci. Technol. 24 (2010) 1083–1095.
[50] Y.Q. Zhu, T. Sekine, Y.H. Li, M.W. Fay, Y.M. Zhao, C.H. Patrick Poa, W.X. Wang, M.J. Roe, P.D. Brown, N. Fleischer, R. Tenne, Shock-Absorbing and Failure Mechanisms of WS_2 and MoS_2 Nanoparticles with Fullerene-like Structures under Shock Wave Pressure, J. Am. Chem. Soc. 127 (2005) 16263–16272.
[51] A.P. Shpak, A.M. Korduban, L.M. Kulikov, T.V. Kryshchuk, N.B. Konig, V.O. Kandyba, XPS studies of the surface of nanocrystalline tungsten disulfide, J. Electron. Spectrosc. Relat. Phenom. 181 (2010) 234–238.
[52] X. Yan, B. Xu, X. Yang, J. Wei, B. Yang, L. Zhao, G. Yang, Through hydrogen spillover to fabricate novel 3DOM-H_xWO_3/Pt/CdS Z-scheme heterojunctions for enhanced photocatalytic hydrogen evolution, Appl. Catal., B 256 (2019) 117812.
[53] J. Chen, D. Yu, W. Liao, M. Zheng, L. Xiao, H. Zhu, M. Zhang, M. Du, J. Yao, WO_{3-x} Nanoplates Grown on Carbon Nanofibers for an Efficient Electrocatalytic Hydrogen Evolution Reaction, ACS Appl. Mat. Interfaces 8 (2016) 18132–18139.